Science
AAAS

Supplementary Materials for

Developmental strategies underlying gigantism and miniaturization in non-avialan theropod dinosaurs

Michael D. D'Emic *et al*.

Corresponding author: Michael D. D'Emic, mdemic@adelphi.edu

Science **379**, 811 (2023)
DOI: 10.1126/science.adc8714

The PDF file includes:

Other Supplementary Material for this manuscript includes the following:

Materials and Methods

Sampling

We assembled a database of non-avialan theropod skeletal histology data from the literature, encompassing over 100 studies that described ca. 200 skeletal elements of over 120 non-avialan taxa from the past several decades (Data S1). We used the phylogeny presented in O'Connor et al. (*39*) in delimiting avialan from non-avialan taxa. From this list, we obtained as many loans as possible of thin sections from museums for re-imaging and re-analysis (excluding those that were lost or currently under study by other researchers). We also obtained loans and permission to re-section bones from as many taxa as possible to produce better quality histological data than was previously published (e.g., *Acrocanthosaurus*), to section the diaphyses of long bones in which original studies had sectioned less optimal and/or non-standardized locations (e.g., the metaphysis of *Saurornitholestes*), or to replace sections that were made but have since been lost (e.g., *Megalosaurus*). All examined specimens are accessioned in publicly accessible repositories. We studied and re-traced all usable published non-avialan theropod thin sections reposited in online databases such as Morphobank or in the online supplemental materials of journal articles. Finally, we conducted novel histological sampling in 10 non-avialan theropod species that had not been examined previously, obtaining multi-element sections when permitted (Data S1). We were not able to include a large dataset from a recent study (*40*) because they were obtained at the microanatomical and not the histological level.

Thin sections were obtained using standard paleo-osteohistological procedures (*4*). Briefly, samples were embedded in epoxy resin, cut to thick sections, mounted on glass or plexiglass with cyanoacrylate, sanded to a thickness of 20–100 microns and polished. High-resolution digital montages were taken on a Zeiss Axioimager using Zen 2.0 software at 50x total

magnification. The tibia of the largest specimen of *Deinonychus* (MCZ 4371) was not available for sectioning, thus it was μCT scanned at Harvard University using the following scan parameters: 170 kV, 106 mA, isotropic voxel size 24.832 cubic microns.

Crushed or broken histological sections were digitally retrodeformed using Adobe Photoshop by aligning cortical bone features such as cracks, staining, growth marks, or endosteal lamellar bone. We traced annual cortical growth marks (i.e., annuli or lines of arrested growth) in Adobe Illustrator. Each digital thin section was independently traced by at least three authors to ensure objectivity and replicability of tracings. Growth marks were used as annual indicators of growth following a wealth of studies demonstrating their periodicity across extant vertebrates (e.g., *41, 42* and references therein). A recent study challenging the utility of cortical growth marks for age estimation (*43*) failed to account for commonly recognized issues of variable medullary expansion as well as tissue shrinkage and deformation in decalcified specimens, which likely explain the differing results they obtained between decalcified and ground sections. cortical growth marks are identified as double or multi-cortical growth marks if they extend along the circumference of the bone with essentially no vascular canals between them. Double/Multi-cortical growth marks have been hypothesized to represent a single growth cycle (*44*); thus we only used the circumference of the innermost cortical growth marks within a double/multi-cortical growth marks in our estimations of body mass (Data S1). High-resolution images and cortical growth marks tracings are reposited to figshare (links provided in Data S1).

Details for each sample

Acrocanthosaurus—

Notes on available sample—We included three individuals of *Acrocanthosaurus* in this study: a partial midshaft cross section from the lateral half of the tibia of NCSM 14345 and the same from OMNH 10146, and one full midshaft cross section from the femur of UM 20796. A fibula and a dorsal rib were also sampled and described in D'Emic et al. (*5*); these were remodeled and so were not useful for growth or longevity estimation and were excluded from this study.

Albertosaurus—

Notes on available sample— Mass was recalculated for *Albertosaurus* using data given by Erickson et al. (*3*) by taking the adult mass for each taxon using the equation of Campione et al. (*45*) applied to the largest known individual in the dataset of Benson et al. (*46*). Masses of smaller individuals were scaled to the larger one by the proportions listed in Erickson et al. (*3*). Masses of multiple individuals of the same age were averaged.

Albinykus—

Notes on available sample—Missing data from a histological sample of the left tibia of *Albinykus* was extrapolated from the dimensions of the right tibia (*47*: fig. 4). We measured the circumferences of cortical growth marks and the endosteal and periosteal borders of this section.

Allosaurus—

Notes on available sample—Data were available for nine individuals of *Allosaurus* (*30, 48, 49*). As noted by Myhrvold (*50*), sampled *Allosaurus* individuals exhibit substantially different growth curves, suggesting taxonomic, individual, sexual, and/or some other differences (e.g., geographic, environmental) among specimens. A

larger dataset and analysis are necessary to explain these differences. Data for three *Allosaurus* specimens were clear outliers (UUVP 30-737, 3164, and 40-264), consisting of very slow growth record at small body size. Since we are interested in maximum growth rates in this study, these slower-growing individuals did not affect our conclusions. We re-traced the cortical growth marks of FMNH P25114 (*30*; pers. comm., T. Cullen, Jan. 2021), finding only 10 instead of the 12 reported cortical growth marks.

Aniksosaurus—

Notes on available sample—Images of the entire section of each of the two tibiae of *Aniksosaurus* sectioned by Ibiricu et al. (*51*) were taken by I. Cerda and cortical growth marks were traced for this study.

Appalachiosaurus—

Notes on available sample—The femur and fibula of the holotype and only known individual of *Appalachiosaurus* (RMM 6670) was sampled as part of this study. Carr et al. (*52*, page 132) commented on the ontogenetic status of the holotype: "A proximal caudal vertebra, still in its field jacket, has a traceable neurocentral suture. A study of neurocentral suture closure, as done for crocodylians (sensu *53*), has not been conducted for tyrannosaurids. Although the ontogenetic sequence of suture closure is unknown for the clade, open sutures suggest RMM 6670 was not an adult at death." However, the regions where all of these sutures are present are damaged; where there is well preserved bone it is finished (i.e., smooth; MDD. pers. obs. 2012). Regardless, as noted by Carr et. al (*52*), the tyrannosaurid pattern of skeletal fusion is unknown, so these data do not inform the ontogenetic status of *Appalachiosaurus*.

A section of the anteromedial face of the midshaft of the left femur was taken. cortical growth marks are preserved in the deep cortex, showing that the growth record pre-onset of the rapid phase of growth is preserved. The circumference of the left femur of RMM 6670 is unavailable, but it is predicted to be 259.5 mm based on the right femur of the same individual (*52*), so this value was used to scale the reconstructed periosteal circumference and cortical growth marks in the incomplete, left femur. A midshaft section of the fibula was also sampled.

Averostra indet. —

Notes on available sample— Evans et al. (*54*) described a noasaurid femur and a femur referable to Averostra (ROM 65779). No cortical growth marks were present in the noasaurid femur and its medullary cavity is exceptionally large, so we excluded it from our study. However, at least five cortical growth marks were reported in the indeterminate averostran. We re-traced the section and found a sixth cortical growth marks, visible deep in the cortex (*54*: fig. 2D).

Ceratosaurus nasicornis—

Notes on available sample—We sampled five bones from four individuals of *Ceratosaurus*: the tibia of MWC.1 (whole cross section), the femur (anterior partial midshaft section) and dorsal rib (whole cross section of the shaft) of BYU 881/12893, the femur of BYU 725/5133 (anterior partial midshaft section), and the dorsal rib of UMNH VP 5278 (whole cross section of the neck). Regarding the latter specimen, a section of the tibia was taken some time in the past, as evidenced by a missing section in the bone, but the section is now lost and permission for additional sampling of the tibia could not be obtained (MDD, pers. obs. 2013).

Coelophysis bauri/*Coelophysis* sp./Coelophysoidea indet.—

Notes on available sample—Eight specimens of *Coelophysis* (six femora and two tibiae) were included in this study (*55–57*). Images of two specimens were provided for study by S. Werning. Though taxonomic opinions have differed over the years concerning these specimens (*57*), the exact taxonomic identification and interrelationships of these specimens are immaterial to our study because of the sparse sample available to us near the base of Theropoda. Therefore, we treat these specimens as a single taxon.

*Cryolophosaurus e*llioti—

Notes on available sample—One partial femoral midshaft section was figured and described in Cullen et al. (*30*). We re-traced cortical growth marks in a high-resolution image of this thin section and identified the same four growth marks.

Daspletosaurus—

Notes on available sample—See *Albertosaurus* above for notes on this taxon, for which we followed the same protocol regarding specimens from Erickson et al. (*3*).

Deinonychus—

Notes on available sample—We histologically sampled one entire midshaft cross section of a femur (MOR 1178) and μCT scanned one tibia (MCZ 4371) of *Deinonychus* for this study. The bone histology of one of these specimens has been reported (the fibula of MOR 1178) along with two other *Deinonychus* specimens (MCZ 8791) and AMNH 3015 (*58–60*). Note that the radial and fibular sections reported by Parsons and Parsons (*58, 59*) are from the metaphyses of the bones, not the midshafts as reported (MDD, pers. obs. 2017; 2019). The radius of MOR 1178

was reported to have an external fundamental system, but firsthand examination of the section reveals that the reported external fundamental system is instead multiple lines of arrested growth and that regions of the thin section adjacent to that shown in the paper (*59*: fig. 3A) indicate a still-growing individual (MDD and TRP pers. obs., 2019).

Eoabelisaurus—

Notes on available sample—A sample was taken of the complete midshaft of the tibia of *Eoabelisaurus* (MPEF PV 3990).

Gorgosaurus—

Notes on available sample—See *Albertosaurus* above for notes on this taxon, for which we followed the same protocol regarding specimens from Erickson et al. (*3*). For the specimen FMNH PR 2211 (*30*), we downloaded the high-resolution slide from the provided Morphobank project and re-traced cortical growth marks.

Halszkaraptor—

Notes on available sample—We downloaded the original synchrotron scans of MPC-D102/109 published by Cau et al. (*61*) and traced the single cortical growth marks and endosteal and periosteal borders around the tibial cortex.

Herrerasaurus—

Notes on available sample—Only a partial section of a *Herrerasaurus* tibia (MCZ 7064; *57*) was available, provided for study by S. Werning. We were able to confidently predict its full circumference at 107 mm via regression based on other more complete specimens (Data S1). A humerus of the same individual has also been sectioned and described (*7, 56, 57, 62*).

Lepidus—

Notes on available sample—Nesbitt and Ezcurra (*63*) depicted a thin section of a femur referred to *Lepidus* (TMM 41936-1.3). The full cross section was taken at the distal-most level of the fourth trochanter and no cortical growth marks were reported. We borrowed the thin section and confirmed the absence of cortical growth marks. We traced the inner and outer borders of the section in Adobe Illustrator, excluding the bulge in the external margin created by the fourth trochanter. We calculated the minimum annual change in mass based on these inner and outer circumferences. Because this section was not taken at midshaft and because the asymptotic body mass of *Lepidus* is unknown, we excluded it from our comparisons.

Majungasaurus—

Notes on available sample—We sampled four bones (dorsal rib, femur, tibia, fibula) from a large specimen of *Majungasaurus* (FMNH PR 2278) and an additional tibia (DMNH EPV.135993) from a young individual for this study. A mid-shaft break of another, larger *Majungasaurus* tibia (FMNH PR 3369) supplemented our histological observations.

Mapusaurus—

Notes on available sample—We included one tibia of *Mapusaurus* (MCF-PVPH-108.67) in our study. Owing to its large size, it was sectioned in four quadrants.

Masiakasaurus—

Notes on available sample—Three femora and two tibiae of *Masiakasaurus* were available for study (*64*).

Megalosaurus—

Notes on available sample— We obtained a partial femoral thin section of *Megalosaurus bucklandii* (OUMNH J.29753b), taken from the lateral aspect of the diaphysis. This bone was already thin sectioned in the early 1980s (section #J.29753b/p1) and was briefly described but not figured by Reid (*65*:27), but that thin section is now lost. We created a new section from this bone.

Mei—

Notes on available sample—We traced cortical growth marks and the endosteal and periosteal margins on a high-resolution image of the tibia of *Mei* (DNHM D2154; *66*).

Ornithomimidae indet.: Bissekty Formation—

Notes on available sample—One midshaft femoral section of an indeterminate ornithomimid (ZIN PH 304/16; *67*) was digitally retrodeformed and its cortical growth marks and endosteal and periosteal margins were traced. Because medullary expansion removed an excessive amount of the growth record, we could not confirm that we had sampled the phase of rapid growth; furthermore, since the asymptotic body mass and precise phylogenetic position of this specimen are unknown, we excluded it from our comparisons.

Ornithomimidae indet.: Horseshoe Canyon Formation—

Notes on available sample—One tibial section (CMN 12070) of those presented in Cullen et al. (*68*) was complete enough for analysis. Because medullary expansion removed an excessive amount of the growth record, we could not confirm that we had sampled the phase of rapid growth; furthermore, since the asymptotic body mass and

precise phylogenetic position of this specimen are unknown, we excluded it from our comparisons.

Quilmesaurus—

Notes on available sample—We sampled the tibia of *Quilmesaurus* (*69*; MPCA-Pv 100), which was substantially crushed and required digital retrodeformation.

"*Raptorex*" *kriegsteini*—

Notes on available sample—The femoral bone histology of a small tyrannosauroid (LH PV 18) that either represents its own genus ("*Raptorex*") or a juvenile of another taxon was described by Sereno et al. (*70*) and Fowler et al. (*71*). The latter study showed that the individual was a juvenile, citing the few, roughly evenly spaced cortical growth marks within the cortex and the general lack of remodeling that would be expected in an older individual. We traced the circumferences of the cortical growth marks indicated in Fowler et al. (*71*:fig. 2A). No scale bar was presented with the published images, so the measured circumference of the entire section was scaled to the value of 87 mm given by Benson et al. (*72*: supplemental information). Because we could not confirm that we had sampled the phase of rapid growth in this very young individual and the asymptotic body mass and precise phylogenetic position of this specimen are unknown, we excluded it from our comparisons.

Rativates evadens—

Notes on available sample—One tibial thin section of *Rativates* (*73*) was digitally retrodeformed and cortical growth marks were traced.

Saurornitholestes langstoni—

Notes on available sample—A tibial section of the dromaeosaurid *Saurornitholestes* was described by Reid (*74*) and its growth was analyzed by Lehman (*75*). We borrowed the specimen and re-examined it, finding that the section prepared by Reid (*74*) and analyzed by Lehman (*75*) was taken at the metaphysis of the tibia. We re-sectioned the bone at its diaphysis, which preserves a more complete record of growth and that can be scaled to body mass.

Shishugounykus inexpectus—

Notes on available sample—Femoral cortical growth marks circumferences reported for *Shishugounykus* (IVPP V23567) by Qin et al. (*35*) were used in this study.

Shuvuuia deserti—

Notes on available sample—One femoral thin section of *Shuvuuia* (IGM 100/unknown) was made available for study by G. M. Erickson; we refrain from a description of the bone histology of this individual since it is still under study, and only report our cortical growth mark tracings and circumferences.

Sinornithomimus dongi—

Notes on available sample—Two tibiae of *Sinornithomimus* were used in this study (LH PV6 "4"; LH PV9 "2"). These were described by Varricchio et al. (*76*) and were digitally retrodeformed and their cortical growth marks traced here.

Spinosaurus aegypticus—

Notes on available sample—One femur of *Spinosaurus* (FSAC-KK 118888) was made available for study by P. Sereno. Only cortical growth mark tracings are presented because the specimen is otherwise still under study.

Suchomimus tenerensis—

Notes on available sample—Two femora of *Suchomimus* (MNN GAD 72, 99) were made available for study by P. Sereno. Only cortical growth mark tracings are presented because the specimens are otherwise still under study.

Tarbosaurus bataar—

Notes on available sample— cortical growth mark circumferences *Tarbosaurus bataar* (MPC-D 107/7) were made available by A. Lee (pers. comm., 2015). Because this is a young juvenile specimen and samples from more mature specimens are unavailable, it was excluded from our comparisons.

Timimus hermani—

Notes on available sample—We obtained an image of a full section of a referred femur of *Timimus hermani* for study from H. Woodward. The specimen was described and illustrated by Chinsamy et al. (*77*: fig. 2) as having at least nine cortical growth marks; ten were apparent to us in the thin section.

Torvosaurus tanneri—

Notes on available sample—We used one tibia, one femur, one fibula, and one dorsal rib of *Torvosaurus* for this study. The long bones were sampled near midshaft and the dorsal rib was sampled at its neck following Waskow and Mateus (*78*). The tibia and fibula may or may not pertain to one individual (BYU 725/2017). The femur and dorsal rib pertain to a single individual (BYU 20697). The tibial section was overlain on a photograph of the broken cross section of the *Torvosaurus* tibia, where the bone delaminated along cortical growth marks allowing them to be traced around the circumference of the section. Only a small core of the femur was available.

Troodon formosus—

Notes on available sample—We used two tibiae of *Troodon* for this study.

Tyrannosaurus rex—

Notes on available sample—Longitudinal data of femora or tibiae were available for four individuals (*30, 55, 79*), and cross-sectional data were available for seven (*3*).

Tyrannotitan chubutensis—

Notes on available sample—We sampled one femur of *Tyrannotitan* (MPEF-Pv 1157) for this study. A subsection of the anteromedial femoral diaphysis was thin sectioned and digitally superimposed onto an image of the broken cross section of the bone, where the thin section was taken. The bone partially delaminated along cortical growth marks while broke, allowing them to be traced around the circumference of the element.

Utahraptor ostrommaysi—

Notes on available sample—One femoral thin section of *Utahraptor* (BYU 7510-15465) was made available for study by G. M. Erickson. Because this femur both has an exceptionally large medullary cavity and is from a very young individual, it was excluded from our comparisons.

Vespersaurus paranaensis—

Notes on available sample—One tibia of *Vespersaurus* (CP/V:4130) was included in our study. Other sections reported in de Souza et al. (*80*) were taken too far from the midshaft/diaphysis to be comparable to the other specimens in our dataset.

Xixianykus zhangi—

Notes on available sample—Femoral cortical growth mark circumferences reported for *Xixianykus* (XMDFEC V0011) by Qin et al. (*35*) were used in this study.

Data Protocols

We capitalized on the available dataset by developing two novel protocols for reliably estimating missing data. First, we performed a sensitivity analysis to observe the effect of missing data and cortical drift (i.e., anteroposteriorly and/or mediolaterally asymmetrical cortical growth and medullary expansion) by digitally simulating hemi-sections from true *Masiakasaurus* sections (*64*) and duplicating a hemi-section of *Appalachiosaurus* (this study; Data S1). Cortical growth marks traced from digital hemi-sections purposely altered to exhibit extreme amounts of cortical drift did not preserve accurate circumference data, but the successive differences in cortical growth mark circumferences were preserved, indicating that growth data are still accessible in partial sections under realistic amounts of cortical drift and only affecting growth data by 1–4%. The femur exhibits more cortical drift than the tibia in non-avialan theropods (*49*), so tibial data are even less affected than the femoral data evaluated here. Thus, we scaled partial circumferences (if at least 1/3 section was available) evident in thin sections to full ones measurable on whole bones (Data S1). Medial or lateral midshaft hemi-sections preserve an unbiased record of growth, which will help increase future datasets since collections managers and curators are generally more amenable to sampling hemi-sections rather than full sections.

Second, we compiled a dataset of non-avialan theropod femoral and tibial circumferences (n = 43) and performed an ordinary least squares regression and a phylogenetic generalized least squares regression using a composite phylogeny scaled to geologic time (Data S2; fig. S1). Femoral and tibial circumferences scale tightly with one another ($p = 7\ e^{-38}$, $r = 0.99$; PGLS regression: ln(tibia circumference) = 1.057*ln(femur circumference) - 0.077; Pagel's lambda ~0.73) and the average percent error predicting one from the other was 8%; this allowed the

transformation of tibial circumferences to femoral ones, with the latter then input into the Campione et al. (*45*) bipedal equation for estimating body mass. Since our aim was to infer the maximum annual growth rate in a taxon, we used fibulae and ribs to constrain whether or not the explosive phase of growth had been achieved by a given individual, since these elements suffer less dense cortical remodeling and medullary expansion than femora or tibiae and have thus been commonly employed for skeletochronology (e.g., *3, 30, 35*). The explosive phase of growth was inferred to be present if a section exhibited narrow spacing between cortical growth marks deep in the cortex, followed by externally more widely spaced marks, followed again by more narrowly spaced marks. A recent study by Cullen et al. (*30*) reported that 'non-weight bearing' bones such as fibulae (which do bear weight) preserved fewer cortical growth marks than 'weight bearing' bones such as tibiae. This observation stands in contrast to our own observations and a number of published studies (e.g., *3, 35*). These conflicting observations may be explained by different sampling locations within bones: histology varies dramatically along the course of tapering bones such as fibulae and ribs, both of which grow asymmetrically in a proximo-distal sense. Within-bone sampling location was not reported in Cullen et al. (*30*).

Available data from fibulae and ribs were not used for mass estimation because they are not sampled in homologous locations among studies—the tapering shafts of these elements mean that slight variations in sampling location would translate to large variances in body mass estimation, unlike the straight-shafted tibiae and femora employed for body mass estimation herein.

Measurement and Estimation of Body Mass and Maximum Annual Growth Rate

Femoral circumference was translated to body mass using the bipedal equation developed by Campione et al. (*45*), scaled using developmental mass extrapolation (DME; *81*) for cortical growth marks deposited before somatic maturity was reached. DME was used instead of direct scaling of cortical growth marks circumferences because the former yields body mass estimates that are concordant with those derived from volumetric models (*82*). DME requires adult body mass to be known; we estimated this when we could, but in several instances we could not, and these samples were excluded from further quantitative analysis (Data S1). Annual percent growth was calculated for every successive pair of cortical growth marks for each section, and the maximum value was recorded as the percent maximum annual growth rate for the species.

Phylogeny Reconstruction

We assembled a composite phylogeny following several recent studies (*35*, *66*, *83*–*87*), including polytomies in uncertain areas. Branch lengths were scaled to geologic time using vetted data from the Paleobiology Database (https://paleobiodb.org) and can be found in Data S1.

Regressions, Ancestral State Reconstruction, and Phylomorphospace

We used the R code provided in D'Emic et al. (*88*) or PAST4 (*89*) to perform regressions. We created a phylomorphospace and performed ancestral state reconstructions using maximum likelihood via the fastAnc function in phytools (*90*). Plots were edited for clarity in Adobe Illustrator. R code and data are provided in Data S2.

Explanation of Columns and Sheets in Data S1 excel file, sheet "DATA"

- Specimen Numbers and Citations: specimen numbers and citations for each sampled element. See sheet “Institutional Abbreviations” for institutional abbreviations listed with specimen numbers.
- Element: which bone was sampled.
- Tibia CGM circ (mm): the circumference of the cortical growth marks (CGM) measured in each tibia, in mm.
- PGLS femur CGM circ estimate (mm): the femoral cortical growth mark circumference that corresponds to each tibial cortical growth mark, using the formula derived from the code in Data S2 and shown in Fig. S1.
- femur CGM circumf being employed (mm): the femoral cortical growth mark circumferences used to estimate body mass for that element. If femoral cortical growth mark circumferences could be measured, those were employed. If tibial cortical growth mark circumferences were measured, they were used to estimate femoral cortical growth mark circumferences.
- direct mass estimate (kg): mass estimate per cortical growth mark based on equation 7 of Campione et al. (*45*).
- % increase in mass/year: annual mass increase expressed as a percentage.
- DME est cubed femur length (cm^3) (Kilbourne & Makovicky 2010): the femur length inferred from “femur CGM circumf being employed (mm)”, cubed, using the equation provided in Kilbourne and Makovicky (*91*).
- DME mass (kg): mass calculated using developmental mass extrapolation (DME; *81*).
- DME increase in mass/year (kg/yr): kg grown per year using DME values.
- DME % increase in mass/year: percentage mass increase per year using DME values.

- Notes: notes on particular taxa that require additional explanation.

Histological descriptions

Below we describe the bone histology of previously unsampled non-avialan theropod taxa and provide notes and additional descriptions for other taxa sampled in our dataset, arranged in alphabetical order by genus. See Data S1 for institutional abbreviations. See figshare links in Data S1 for histological montages and cortical growth mark tracings.

Acrocanthosaurus—

Histological description—D'Emic et al. (*5*) provided a detailed description of the bone histology of *Acrocanthosaurus* which will not be repeated here, but a few notes are warranted. First, D'Emic et al. (*5*) cited a count of eleven cortical growth marks (in the form of lines of arrested growth) for the tibia of NCSM 14345 and OMNH 10146 based on observations of portions of the full available sections. New observations indicate that these tibiae exhibit eight and 14 lines of arrested growth because some lines of arrested growth cited by D'Emic et al. (*5*) represent double lines. Second, we note that our results differ from those of Cullen et al. (*30*), because those authors did not include adult sections of *Acrocanthosaurus* described by D'Emic et al. (*5*) in making their comparisons, citing only data from the described juvenile section.

Albertosaurus—

Histological description—See Erickson et al. (*3*).

Albinykus—

Histological description—See Nesbitt et al. (*47*). Because of the very small size of the circumferences, the regression equation could not be used to convert tibial to femoral circumferences. However, the femur and tibia are identical in diameter (*47*: fig. 2), so tibial circumferences were substituted for femoral ones.

Allosaurus—

Histological description—See Bybee et al. (*48*).

Aniksosaurus—

Histological description—See Ibiricu et al. (*51*).

Appalachiosaurus—

Histological description— The femur consists of a well-vascularized cortex of mostly woven bone with small amounts of parallel-fibered bone, increasing in proportion towards the periosteal border. Vascularity is more circumferential internally and predominantly longitudinal externally. Scant secondary osteons are present near the endosteal margin, where a thick layer of poorly vascularized lamellar endosteal bone lines the medullary cavity. The fibula is nearly completely remodeled, with at least five cortical growth marks present externally but no external fundamental system.

Averostra indet. —

Histological description—See Evans et al. (*54*).

Ceratosaurus nasicornis—

Histological description—

MWC.1—The tibia of this specimen pertains to a relatively small individual of *Ceratosaurus*—with the femur and tibia of this individual at 630 mm and 520 mm long, respectively (*92*). The neural arches are fused to their respective centra and the tibiotarsal elements are fused to one another (*92*). The individual has been interpreted as a juvenile based on the lack of fusion among cranial bones (*92*), though many bones are not fused to one another in a much larger individual (UMNH VP 5278) as well. The tibial thin section is crushed, leaving no medullary cavity. The tibial cortex is composed of mostly parallel-fibered to woven bone with plexiform vascularity that is slightly more circumferential in the external part of the section. An external fundamental system is present.

BYU 881/12893—This femur of BYU 881/12893 pertains to the largest known for *Ceratosaurus* (*93*), with a midshaft circumference of 275 mm. The section is comprised of parallel fibered to woven bone with plexiform vascularity. Secondary remodeling is scattered throughout the section, generally denser internally but locally extending to the outermost edge of the bone and few areas have dense or overlapping secondary osteons. The inner edge of the section is lined with a ca. 0.5 mm thick layer of endosteal parallel-fibered to lamellar bone. Cortical growth marks are absent through the cortex until the external edge, where an external fundamental system is present.

The section of the dorsal rib of BYU 881/12893 is nearly completely remodeled; the cortex grades gradually into a relatively small and dense medullary cavity. An external fundamental system is present. Enough primary bone is visible internally to show that no cortical growth marks are present in the deep cortex, as in the femur. Primary vascular canals are longitudinal in orientation, and primary bone is parallel-fibered or woven.

BYU 725/5133—This femur pertains to one of the smallest *Ceratosaurus* individuals known, with a midshaft circumference of 219 mm. The cortex consists of nearly all primary bone that is parallel-fibered or woven in organization interspersed with plexiform vascularity. Internally, the medullary cavity is lined with ca. 0.25 mm of nearly avascular, endosteal lamellar to parallel-fibered bone. Externally, staining obscures some details of the periosteal margin, but no apparent change in bone tissue organization or vascularity is apparent. No external fundamental system is present.

UMNH VP 5278—The femur and tibia of this individual are 735 mm and 635 mm long, respectively (MDD pers. obs. 2013), making it one of the larger *Ceratosaurus* individuals in our dataset. The neurocentral sutures, scapulocoracoid, and the tibiotarsal elements are fused (*92*). The section of the dorsal rib of UMNH VP 5278 has a large medullary cavity lined by a substantial ring of endosteal lamellar bone (also visible in *94*: fig. 74). The bone is mostly remodeled. The periosteal border exhibits tightly spaced growth lines indicative of an external fundamental system. There are three cortical growth marks between the endosteal border and the external fundamental system on the posterior face of the section. Vascular orientation is

primarily longitudinal and bone tissue organization is primarily parallel-fibered or woven.

Coelophysis bauri/*Coelophysis* sp./Coelophysoidea indet.—

Histological description—See (*55*–*57*). Each sub-sample (*C. bauri*, *C.* sp, Coelophysoidea indet.) has exceptionally high maximum annual growth rates (Data S1). Note that UCMP 129618 does not preserve cortical growth marks, so its inner and outer cortical circumferences were measured to provide a minimum estimate of bone growth in one year. The exceptionally high maximum annual growth rate inferred in *Coelophysis* is consistent with the conclusions of other studies that describe its histology (*56*).

*Cryolophosaurus e*llioti—

Histological description—See Cullen et al. (*30*).

Daspletosaurus—

Histological description—See Erickson et al. (*3*).

Deinonychus—

Histological description—

MOR 1178—The femur of MOR 1178 is roughly circular in cross section, as is its substantial medullary cavity. The abundant vascularization is mostly reticular to circumferential in organization. The fibrolamellar bone tissue contains a substantial

amount of woven bone. Cortical growth marks are abundant in the form of single and double lines of arrested growth. No external fundamental system is present.

MCZ 4371—The μCT section of MCZ 4371 reveals fine histological details including vascular canals, but the type of bone tissue could not be ascertained due to resolution limits. Remodeling is abundant around the perimeter of the oval medullary cavity, and substantial resorption occurred towards the lateral margin of the inner cortex. Cortical growth marks are evident towards the outer half of the cortex, where they quickly decrease in spacing towards the periosteum.

Eoabelisaurus—

Histological description—The tibial cortex is well vascularized, consisting of fibrolamellar bone with mostly circumferential vascularization. Some remodeling and resorption are evident near the medial and lateral portions of the inner cortex. The bone exhibits ten roughly regularly spaced growth cortical growth marks and no external fundamental system. A thin band of avascular, lamellar endosteal bone lines the medullary cavity.

Gorgosaurus—

Histological description—See Erickson et al. (*3*).

Halszkaraptor—

Histological description—See Cau et al. (*61*).

Herrerasaurus—

Histological description—The humeral section contains only one cortical growth mark and perhaps lacks an external fundamental system, but its surface is abraded. In contrast, the tibia of MCZ 7064 has no cortical growth marks outside the external fundamental system (*57*), indicating that it grew quickly and was at somatic maturity.

Lepidus—

Histological description—See Nesbitt and Ezcurra (*63*).

Majungasaurus—

Histological description—

FMNH PR 2278—

Dorsal rib—The section of the neck of the dorsal rib is nearly completely remodeled, with at most a couple of millimeters of primary bone visible in the cortex. The little primary bone that is visible is parallel-fibered in organization with mostly longitudinal vascular canals. No open or spongy medullary cavity is present. Fourteen lines of arrested growth are present and not arranged concentrically around the margin of the bone, indicating asymmetric growth.

Femur—The femoral section preserves the medial, lateral, and posterior faces of the bone. Remodeling occupies about half of the medial and lateral cortex, whereas posteriorly, dense remodeling extends all the way to the periosteal margin. Approximately 11 lines of arrested growth are present in this section, many of which are multi-lines of arrested growth . The spacing of

the lines of arrested growth decreases towards the perimeter of the bone, though no external fundamental system is present, indicating that individual was approaching but not at asymptotic size. Primary bone of the femur is parallel-fibered with a small lamellar component. Vascular canal orientation is a combination of longitudinal (more prevalent externally and medially in the section) and circumferential (more prevalent internally and laterally). Remodeling grades into, obscures, or parallels lines of arrested growth in some places. The cortical-medullary boundary is sharp and lined with parallel-fibered to lamellar tissue of low vascularity. Deep to this tissue within the bone on its posterior side is a small piece of tissue of high vascularity, as is found in the tibial section of this individual, but we cannot confirm that it is in situ.

Tibia—A complete midshaft tibial section was taken. Remodeling occupies most of the anterior and lateral parts of the cortex, but is rare otherwise, even near the endosteal margin. Fifteen lines of arrested growth are present in this section, with many being multi-lines of arrested growth as in the femur. Primary bone in the tibial cortex is woven to parallel-fibered in organization. Vascular canal orientation is mainly circumferential, generally moreso than in the femur, but includes some longitudinally oriented canals that increase dramatically in relative proportion near the periosteal margin. As in the femur, remodeling grades into, obscures, or parallels lines of arrested growth in some places. Internal to the lateral part of the endosteal margin is a small rind of bone with a high proportion of irregularly oriented vascular

canals. If this tissue represents medullary bone, it would indicate that this individual was female and sexually mature, but this interpretation awaits confirmation via other data (e.g., *95*). Externally, two rinds of bone extend the surface of the tibia, one from the anteromedial face and another from the anterolateral face, interrupting the gentle curvature of the underlying lines of arrested growth in these regions. This bone is higher in vascularization than that of the underlying cortex, and that vascularization is longitudinal to radial in organization, in stark contrast to the underlying, predominantly circumferential orientation of vascular canals. Periosteal reactive bone with a 'sunburst' vascular pattern consisting of short spicules and the presence of lesions in the lateral part of the bony cortex of the tibia and fibula of *Majungasaurus* match those of an adult *Stegosaurus* tibia (*96*: fig. 1G), suggesting osteomyelitis (i.e., infectious abscess) and/or hypertrophic osteopathy (*97*). The tibial periosteal reactive bone is found on the anterolateral and posterolateral sections of the bone, suggesting that perhaps the infection was localized in that bone to the entheses of intercrural ligaments, whereas similar reactive bone in the fibula (see below) is found laterally, suggesting infection near or at the origin of the fibularis longus and/or brevis muscles (*98*).

Fibula—The fibular cross section lacks a medullary cavity and is nearly completely remodeled. The scant visible primary bone is characterized by lamellar and parallel-fibered tissue organization and almost exclusively longitudinally oriented vascularization. As in the femur and tibia, several

multi-lines of arrested growth are present. In the non-remodeled part of the cortex, preserved anteriorly and laterally, lines of arrested growth quickly decrease in their spacing, towards the periosteum, but neither tissue organization nor the density or orientation of vascular canals decreases between these lines of arrested growth. This is uncharacteristic of an external fundamental system, in which these features usually change in the periosteal direction with the decrease in spacing between lines of arrested growth (*99, 100*).

As described in the tibia, the fibula shows evidence of pathological bone, which appears in surficial and histological views as an irregularly crenulated surface. A rind of bone lines the lateral face of the section, consisting of large erosion rooms, longitudinally oriented secondary osteons, and a mixture of radially and longitudinally oriented primary osteons. The pathological bone grades into normal-looking cortical bone anteriorly.

DMNH EPV.135993—The tibial section of this bone is composed of primarily woven bone with abundant plexiform to circumferentially oriented vascularity. A few cortical growth marks are present in the bone, none of them are multi-lines of arrested growth as in the larger individual (FMNH PR 2278). The lateral face of the bone, which would articulate with the fibula via the interosseus ligament, is heavily remodeled, in contrast to the absence of remodeling elsewhere. The medullary cavity is bounded by a thin layer of avascular endosteal lamellar bone that thickens laterally.

FMNH PR 3369—A diaphyseal break in this tibia reveals many tightly spaced lines of arrested growth (Fig. S5). We did not thin section or trace cortical growth marks in this individual, but it is obvious that its slow annual growth was similar to the other specimens of *Majungasaurus*.

Mapusaurus—

Histological description—The tibial section reveals a large, oval medullary cavity lined by fragments of endosteal lamellar bone. The bone tissue is fibrolamellar, with mostly circumferential vascular organization. No cortical growth marks are observed deep in the cortex; they suddenly appear towards the periosteal margin to culminate in an external fundamental system.

Masiakasaurus—

Histological description—See Lee and O'Connor (*64*).

Megalosaurus—

Histological description—Reticular vascularity predominates in the tibial cortex, composed primarily of woven bone. Scattered remodeling and concentrated resorption are present near the medullary cavity. Only one cortical growth mark is present deep in the cortex, with six near the periosteal edge. Though tightly spaced, the presence of abundant vascularity indicates that they do not represent an external fundamental system.

Mei—

Histological description—See Gao et al. (*66*).

Ornithomimidae indet.: Bissekty Formation—

Histological description—See Skutschas et al. (*67*).

Ornithomimidae indet.: Horseshoe Canyon Formation—

Histological description—See Cullen et al. (*68*).

Quilmesaurus—

Histological description—The bone histology of *Quilmesaurus* was described briefly in a conference abstract (*69*). Poor preservation limits the observation of the bone histology of *Quilmesaurus* to certain regions. In those regions, subequally spaced cortical growth marks bound zones of dense, circumferentially oriented vascularization within mostly parallel-fibered bone tissue. Strips of avascular endosteal lamellar bone delaminated from the inner margin of the cortex. Substantial cortical bone remodeling occupies the innermost medial and lateral sections of the bone. See also Baiano and Cerda (*69*).

"*Raptorex*" *kriegsteini*—

Histological description—See Fowler et al. (*71*).

Rativates evadens—

Histological description—See McFeeters et al. (*73*).

Saurornitholestes langstoni—

Histological description—Our new histological section has a relatively small medullary cavity sharply bounded by a thick layer of avascular endosteal lamellar bone. Remodeling is extensive in the inner half of the cortex. In the outer half of the cortex, longitudinal canals with some anastomoses predominate. The majority of the primary bone is parallel-fibered. Growth lines decrease quickly in spacing towards the periosteal margin to form an external fundamental system.

Shishugounykus inexpectus—

Histological description—see Qin et al. (*35*).

Shuvuuia deserti—

Histological description—See Erickson et al. (*6*).

Sinornithomimus dongi—

Histological description—See Varricchio et al. (*76*).

Spinosaurus aegypticus—

Histological description—See Ibrahim et al. (*101*).

Suchomimus tenerensis—

Histological description—See Ibrahim et al. (*101*).

Tarbosaurus bataar—

Histological description—See Tsuihiji et al. (*102*).

Timimus hermani—

Histological description—see Chinsamy et al. (*77*) and Chinsamy et al. (*103*).

Torvosaurus tanneri—

Histological description—

BYU 725/2017—The tibial cortex is sharply delimited from a small, circular medullary cavity with no sign of endosteal lamellar bone lining it. The inner 1/7th of the tibial cortex has plexiform vascularity whereas the bulk of the cortex has circumferentially (or locally longitudinally) oriented vascularity. The inner region of plexiform vascularity is composed of woven bone, whereas in the circumferential region the bone tissue is parallel fibered with a minor lamellar component. Remodeling is relatively dense in the inner one-fourth of the section. No cortical growth marks are present in the deep cortex and only three lines of arrested growth are present in the outer cortex (one single and two double lines of arrested growth). The fibula is heavily remodeled. Primary bone is mostly parallel-fibered in organization with a minor lamellar component. Vascularization is mostly longitudinal with a few regions dominated by radial canals.

BYU 20697—the femoral core possesses similar inner plexiform and outer circumferential vascularity as the tibial one. Remodeling is sparse and limited to the innermost portion of the section. Like the tibia of the other individual, few cortical growth marks are present. The dorsal rib is heavily remodeled; remaining primary bone consists of lamellar and parallel-fibered bone with longitudinal vascularization.

Troodon formosus—

Histological description—See Varricchio et al. (*104*, *105*).

Tyrannosaurus rex—

Histological description—See Erickson et al. (*3*), Lee (*55*), and Horner and Padian (*79*).

Tyrannotitan chubutensis—

Histological description—Unlike most large-bodied non-avialan theropods, vascularization in *Tyrannotitan* is primarily longitudinal in orientation. Poor preservation makes identification of bone tissue type difficult. Cortical growth marks are somewhat regularly spaced in the bone, becoming slightly closer together near the periosteal margin.

Utahraptor ostrommaysi—

Histological description—See Erickson et al. (*23*).

Vespersaurus paranaensis—

Histological description—see de Souza et al. (*80*).

Xixianykus zhangi—

Histological description—See Qin et al. (*35*).

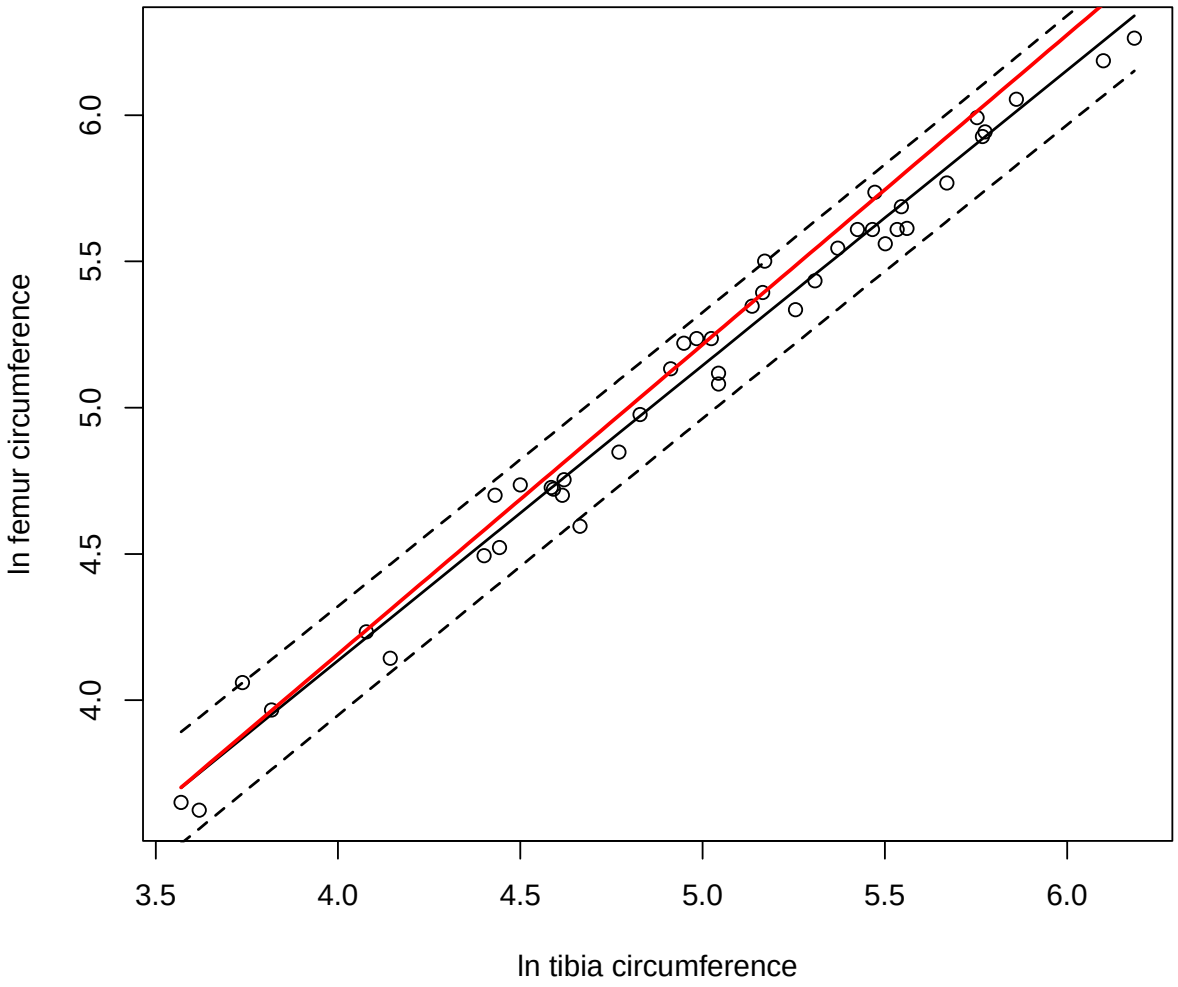

Fig. S1.

Tibial and femoral circumferences (ln scale in mm) scale tightly with one another in non-avialan theropods. Phylogenetic generalized least squares regression (red line) and ordinary least squares regression (black line; dashed lines = 95% confidence intervals). See Data S2 for code and data.

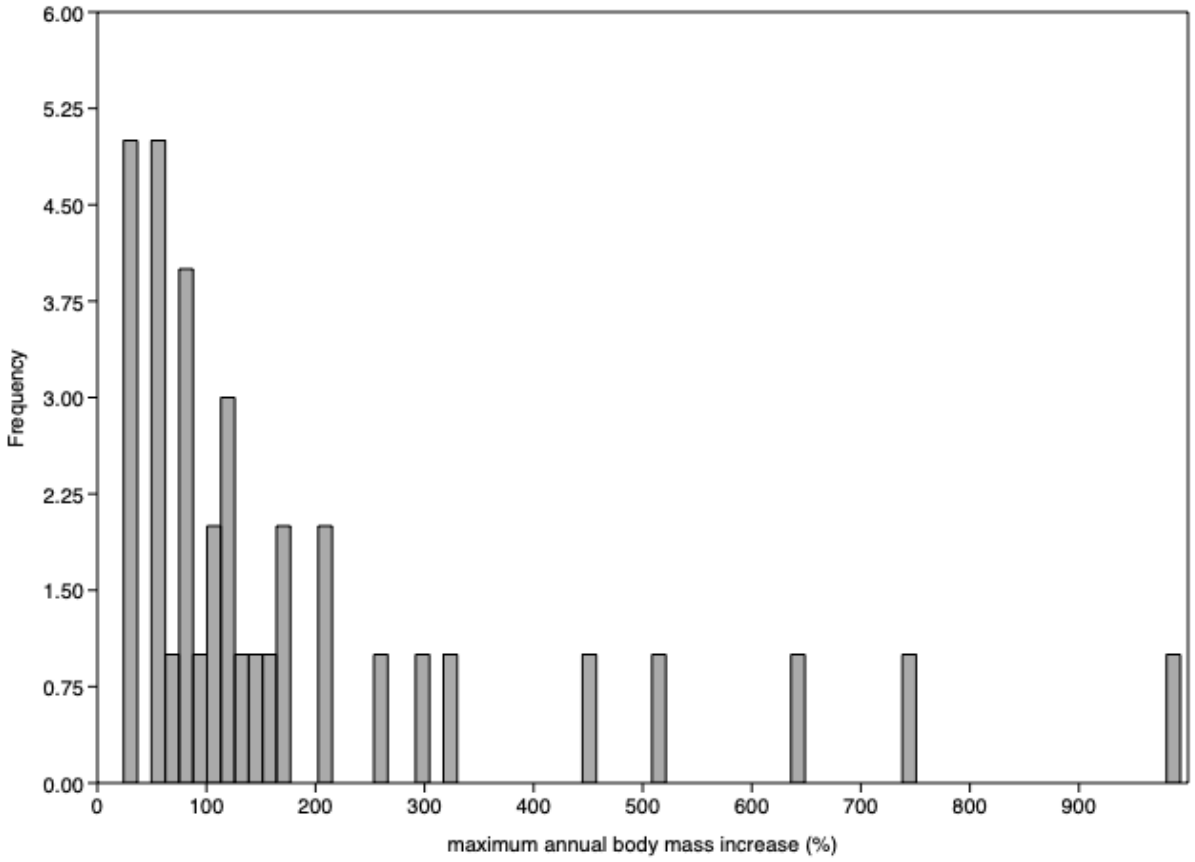

Fig. S2.

Distribution of maximum annual growth rates in a sample of 36 non-avialan theropods.

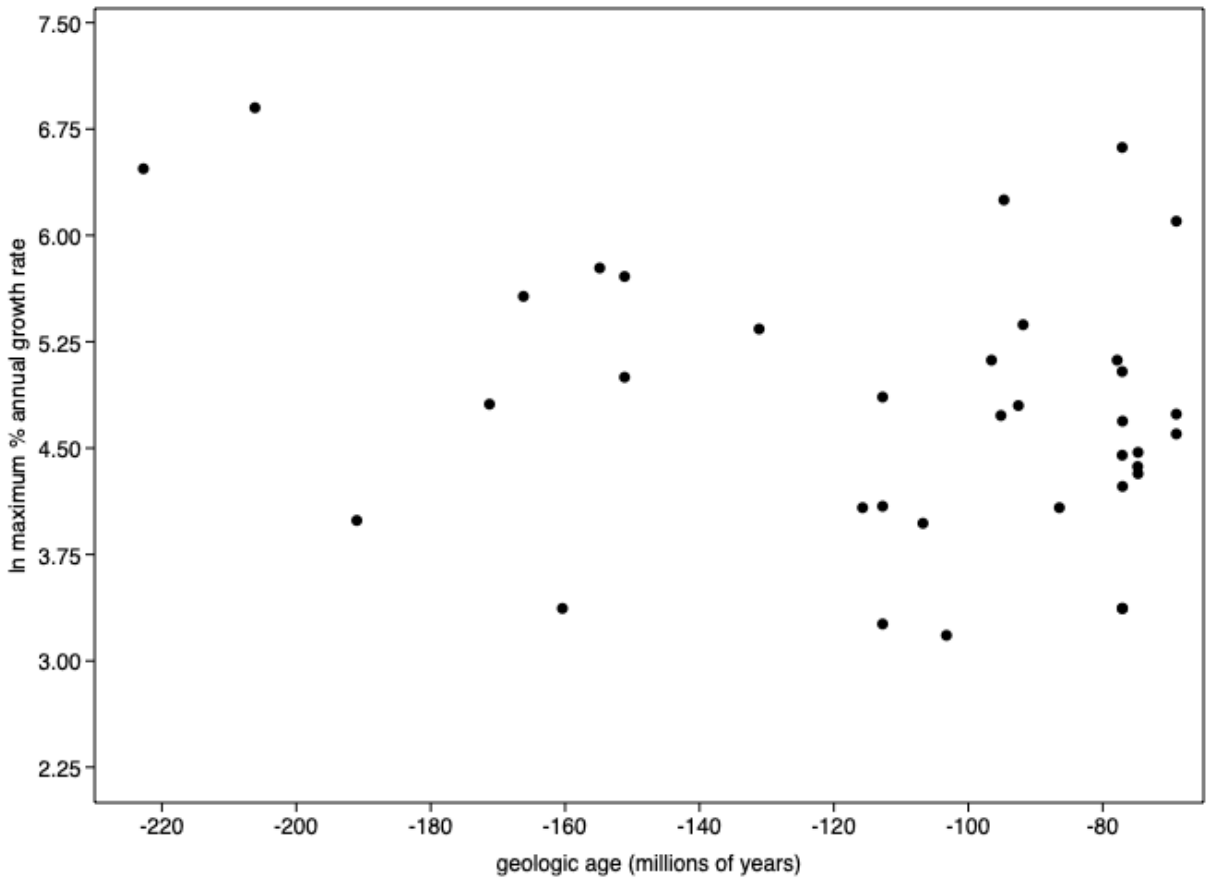

Fig. S3.

Non-avialan theropod maximum annual growth rate through time. Non-avialan theropods exhibit no statistically significant change in maximum annual growth rate throughout their evolutionary history ($r = 0.3$; $p = 0.07$).

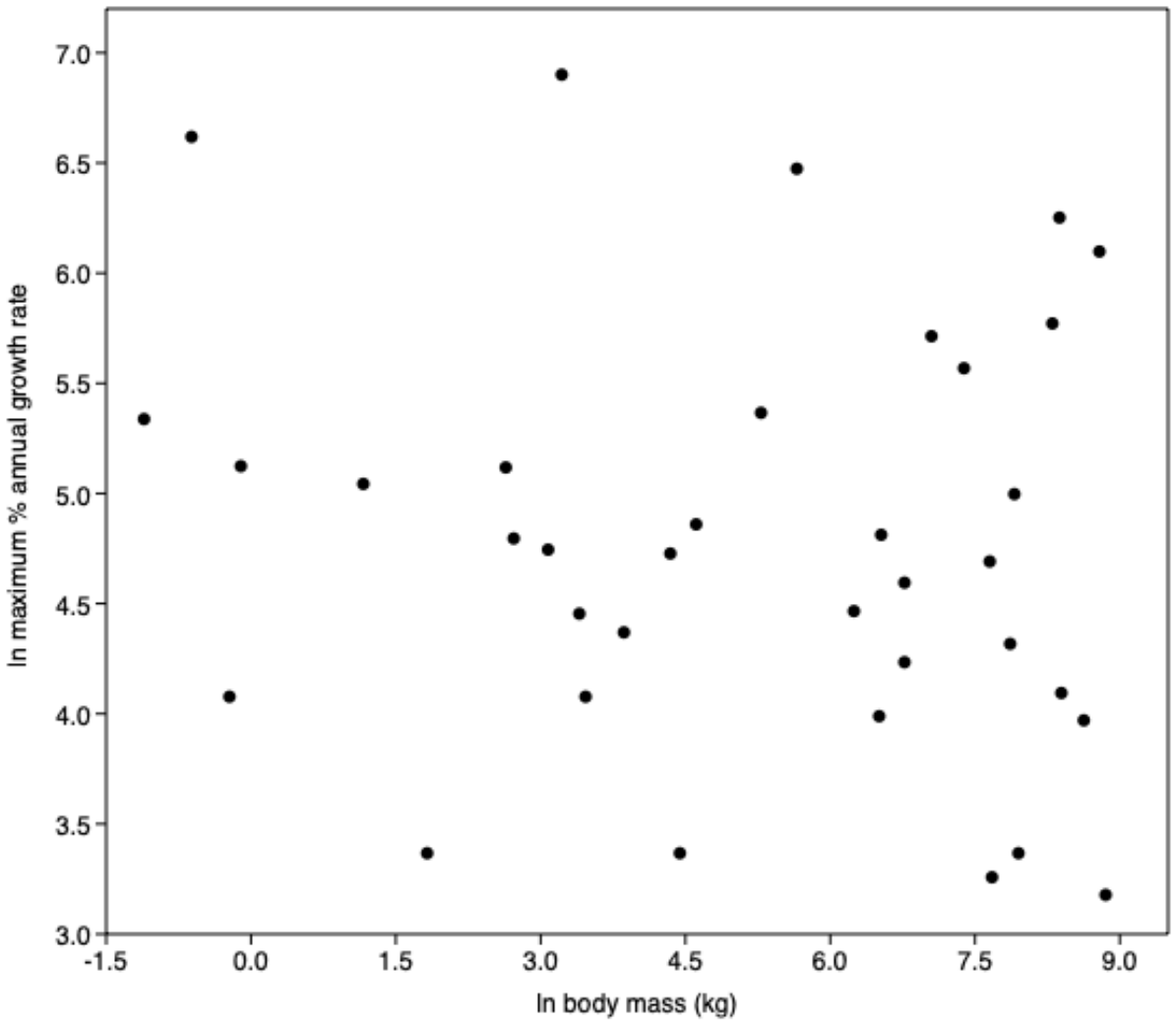

Fig. S4.

Body mass and maximum annual growth rate are unrelated in non-avialan theropod dinosaurs (r = 0.02; p = 0.38).

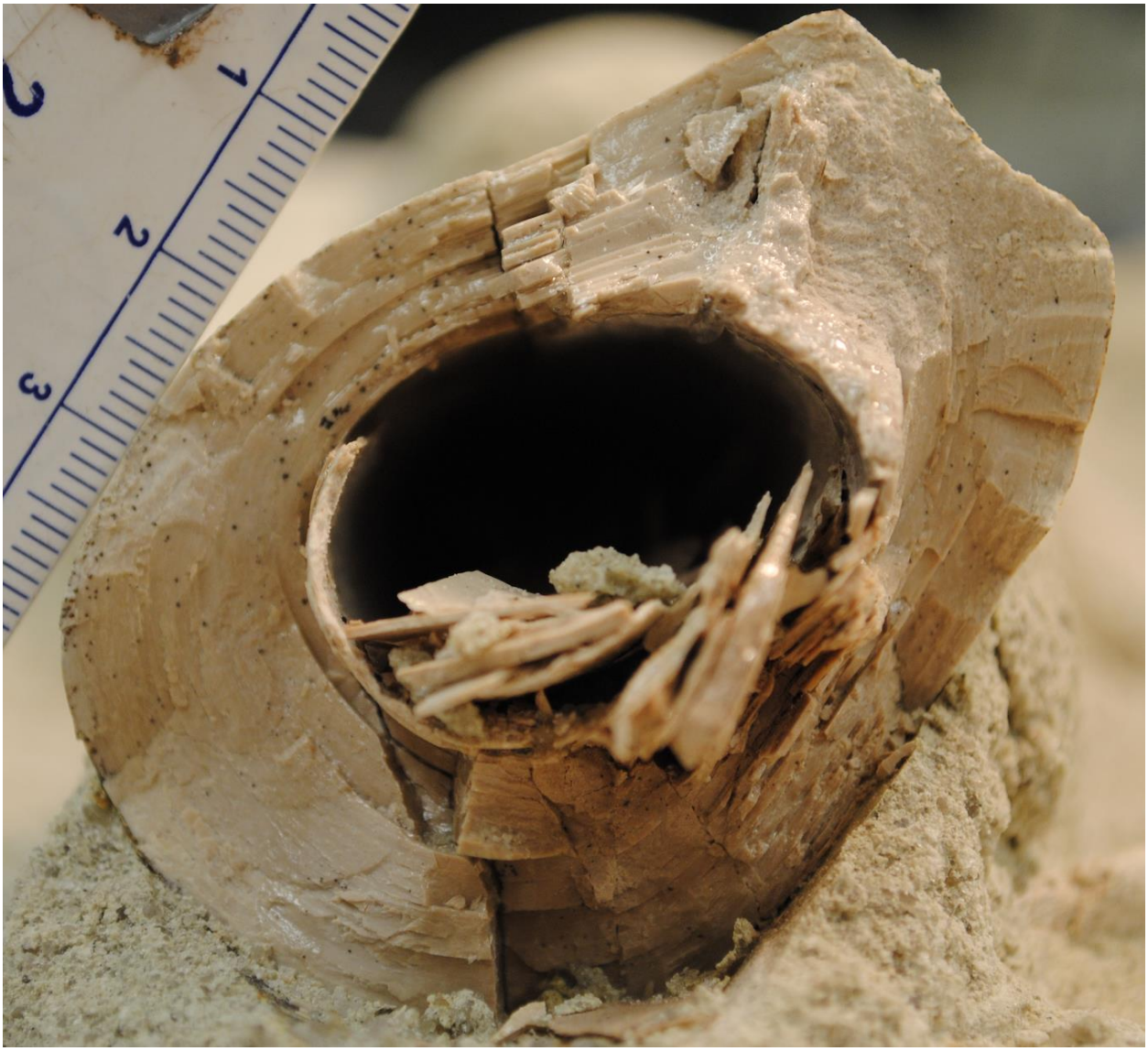

Fig. S5.

A diaphyseal break of an un-sectioned *Majungasaurus* tibia (FMNH PR 3369) reveals tightly spaced cortical growth marks.

Data S1. (separate file)

Microsoft Excel file containing all raw data, a list of sampled specimens, summarized annual growth data, a database of publications from the literature (with citations, specimen numbers, and institutional abbreviations), taxon geologic ages (vetted after gathering from the Paleobiology Database); regression data for Herrerasauridae, growth data for *Alligator*, our validation of use of partial sections showing the negligible effect of missing data and cortical drift, figshare links for high-resolution histological images, and phylopic licenses.

Data S2 (separate zipped file). All R code and associated datafiles necessary to create regressions, ancestral state reconstructions, and phylomorphospace.

References and Notes

1. P. Alberch, S. J. Gould, G. F. Oster, D. B. Wake, Size and shape in ontogeny and phylogeny. *Paleobiology* **5**, 296–317 (1979). doi:10.1017/S0094837300006588

2. K. Padian, A. J. de Ricqlès, J. R. Horner, Dinosaurian growth rates and bird origins. *Nature* **412**, 405–408 (2001). doi:10.1038/35086500 Medline

3. G. M. Erickson, P. J. Makovicky, P. J. Currie, M. A. Norell, S. A. Yerby, C. A. Brochu, Gigantism and comparative life-history parameters of tyrannosaurid dinosaurs. *Nature* **430**, 772–775 (2004). doi:10.1038/nature02699 Medline

4. K. E. J. Chapelle, J. Botha, J. N. Choiniere, Extreme growth plasticity in the early branching sauropodomorph Massospondylus carinatus. *Biol. Lett.* **17**, 20200843 (2021). doi:10.1098/rsbl.2020.0843 Medline

5. M. D. D'Emic, K. M. Melstrom, D. R. Eddy, Paleobiology and geographic range of the large-bodied Cretaceous theropod dinosaur Acrocanthosaurus atokensis. *Palaeogeogr. Palaeoclimatol. Palaeoecol.* **333–334**, 13–23 (2012). doi:10.1016/j.palaeo.2012.03.003

6. G. M. Erickson, K. C. Rogers, S. A. Yerby, Dinosaurian growth patterns and rapid avian growth rates. *Nature* **412**, 429–433 (2001). doi:10.1038/35086558 Medline

7. K. Padian, J. R. Horner, A. de Ricqlès, Growth in small dinosaurs and pterosaurs: The evolution of archosaurian growth strategies. *J. Vertebr. Paleontol.* **24**, 555–571 (2004). doi:10.1671/0272-4634(2004)024[0555:GISDAP]2.0.CO;2

8. R. Redelstorff, P. M. Sander, Long and girdle bone histology of Stegosaurus: Implications for growth and life history. *J. Vertebr. Paleontol.* **29**, 1087–1099 (2009). doi:10.1671/039.029.0420

9. P. Sander *et al*., Adaptive radiation in sauropod dinosaurs: Bone histology indicates rapid evolution of giant body size through acceleration. *Org. Divers. Evol.* **4**, 165–173 (2004). doi:10.1016/j.ode.2003.12.002

10. K. Stein, Z. Csiki, K. C. Rogers, D. B. Weishampel, R. Redelstorff, J. L. Carballido, P. M. Sander, Small body size and extreme cortical bone remodeling indicate phyletic dwarfism in Magyarosaurus dacus (Sauropoda: Titanosauria). *Proc. Natl. Acad. Sci. U.S.A.* **107**, 9258–9263 (2010). doi:10.1073/pnas.1000781107 Medline

11. T. M. Lehman, H. N. Woodward, Modeling growth rates for sauropod dinosaurs. *Paleobiology* **34**, 264–281 (2008). doi:10.1666/0094-8373(2008)034[0264:MGRFSD]2.0.CO;2

12. M. Köhler, S. Moyà-Solà, Physiological and life history strategies of a fossil large mammal in a resource-limited environment. *Proc. Natl. Acad. Sci. U.S.A.* **106**, 20354–20358 (2009). doi:10.1073/pnas.0813385106 Medline

13. S. Herrera-Álvarez, E. Karlsson, O. A. Ryder, K. Lindblad-Toh, A. J. Crawford, How to make a rodent giant: Genomic basis and tradeoffs of gigantism in the Capybara, the world's largest rodent. *Mol. Biol. Evol.* **38**, 1715–1730 (2021). doi:10.1093/molbev/msaa285 Medline

14. E. S. Long, K. L. Courtney, J. C. Lippert, C. M. Wall-Scheffler, Reduced body size of insular black-tailed deer is caused by slowed development. *Oecologia* **189**, 675–685 (2019). doi:10.1007/s00442-019-04367-3 Medline

15. M. Köhler, V. Herridge, C. Nacarino-Meneses, J. Fortuny, B. Moncunill-Solé, A. Rosso, R. Sanfilippo, M. R. Palombo, S. Moyà-Solà, Palaeohistology reveals a slow pace of life for the dwarfed Sicilian elephant. *Sci. Rep.* **11**, 22862 (2021). doi:10.1038/s41598-021-02192-4 Medline

16. A. Ozgul, S. Tuljapurkar, T. G. Benton, J. M. Pemberton, T. H. Clutton-Brock, T. Coulson, The dynamics of phenotypic change and the shrinking sheep of St. Kilda. *Science* **325**, 464–467 (2009). doi:10.1126/science.1173668 Medline

17. G. Orlandi-Oliveras, C. Nacarino-Meneses, G. D. Koufos, M. Köhler, Bone histology provides insights into the life history mechanisms underlying dwarfing in hipparionins. *Sci. Rep.* **8**, 17203 (2018). doi:10.1038/s41598-018-35347-x Medline

18. G. M. Erickson, A. J. de Ricqlès, V. de Buffrénil, R. E. Molnar, M. K. Bayless, Vermiform bones and the evolution of gigantism in Megalania—How a reptilian fox became a lion. *J. Vertebr. Paleontol.* **23**, 966–970 (2003). doi:10.1671/23

19. G. M. Erickson, C. A. Brochu, How the 'terror crocodile' grew so big. *Nature* **398**, 205–206 (1999). doi:10.1038/18343

20. A. K. Huttenlocker, J. Botha-Brink, Bone microstructure and the evolution of growth patterns in Permo-Triassic therocephalians (Amniota, Therapsida) of South Africa. *PeerJ* **2**, e325 (2014). doi:10.7717/peerj.325 Medline

21. A. Chinsamy, A. Elzanowski, Bone histology. Evolution of growth pattern in birds. *Nature* **412**, 402–403 (2001). doi:10.1038/35086650 Medline

22. S. T. Turvey, O. R. Green, R. N. Holdaway, Cortical growth marks reveal extended juvenile development in New Zealand moa. *Nature* **435**, 940–943 (2005). doi:10.1038/nature03635 Medline

23. G. M. Erickson, O. W. Rauhut, Z. Zhou, A. H. Turner, B. D. Inouye, D. Hu, M. A. Norell, Was dinosaurian physiology inherited by birds? Reconciling slow growth in *archaeopteryx*. *PLOS ONE* **4**, e7390 (2009). doi:10.1371/journal.pone.0007390 Medline

24. V. M. Savage, A. P. Allen, J. H. Brown, J. F. Gillooly, A. B. Herman, W. H. Woodruff, G. B. West, Scaling of number, size, and metabolic rate of cells with body size in mammals. Proc. *Natl. Acad. Sci. U.S.A.* **104**, 4718–4723 (2007). doi:10.1073/pnas.0611235104 Medline

25. M. D. D'Emic, R. B. J. Benson, Measurement, variation, and scaling of osteocyte lacunae: A case study in birds. *Bone* **57**, 300–310 (2013). doi:10.1016/j.bone.2013.08.010 Medline

26. G. M. Erickson, On dinosaur growth. *Annu. Rev. Earth Planet. Sci.* **42**, 675–697 (2014). doi:10.1146/annurev-earth-060313-054858

27. T. J. Case, On the evolution and adaptive significance of postnatal growth rates in the terrestrial vertebrates. *Q. Rev. Biol.* **53**, 243–282 (1978). doi:10.1086/410622 Medline

28. J. M. Starck, R. E. Ricklefs, in *Avian Growth and Development: Evolution Within the Altricial Precocial Spectrum*, J. M. Starck, R. E. Ricklefs, Eds. (Oxford Univ. Press, 1998) ch. 1.

29. J. R. Horner, K. Padian, A. de Ricqlès, How dinosaurs grew so large—And so small. *Sci. Am.* **293**, 56–63 (2005). doi:10.1038/scientificamerican0705-56 Medline

30. T. M. Cullen, J. I. Canale, S. Apesteguía, N. D. Smith, D. Hu, P. J. Makovicky, Osteohistological analyses reveal diverse strategies of theropod dinosaur body-size evolution. *Proc. Biol. Sci.* **287**, 20202258 (2020). doi:10.1098/rspb.2020.2258 Medline

31. C. T. Griffin, S. J. Nesbitt, Anomalously high variation in postnatal development is ancestral for dinosaurs but lost in birds. Proc. *Natl. Acad. Sci. U.S.A.* **113**, 14757–14762 (2016). doi:10.1073/pnas.1613813113 Medline

32. J. Cubo, N. Le Roy, C. Martinez-Maza, L. Montes, Paleohistological estimation of bone growth rate in extinct archosaurs. *Paleobiology* **38**, 335–349 (2012). doi:10.1666/08093.1

33. G. Grigg, J. Nowack, J. E. P. W. Bicudo, N. C. Bal, H. N. Woodward, R. S. Seymour, Whole-body endothermy: Ancient, homologous, and widespread among the ancestors of mammals, birds and crocodylians. *Biol. Rev.* (2021). Medline

34. M. S. Y. Lee, A. Cau, D. Naish, G. J. Dyke, Morphological clocks in paleontology, and a mid-Cretaceous origin of crown Aves. *Syst. Biol.* **63**, 442–449 (2014). doi:10.1093/sysbio/syt110 Medline

35. Z. Qin, Q. Zhao, J. N. Choiniere, J. M. Clark, M. J. Benton, X. Xu, Growth and miniaturization among alvarezsauroid dinosaurs. *Curr. Biol.* **31**, 3687–3693.e5 (2021). doi:10.1016/j.cub.2021.06.013 Medline

36. J. I. Canale, F. E. Novas, L. Salgado, R. A. Coria, Cranial ontogenetic variation in Mapusaurus roseae (Dinosauria: Theropoda) and the probable role of heterochrony in carcharodontosaurid evolution. *Palaontol. Z.* **89**, 983–993 (2015). doi:10.1007/s12542-014-0251-3

37. B. A. S. Bhullar, J. Marugán-Lobón, F. Racimo, G. S. Bever, T. B. Rowe, M. A. Norell, A. Abzhanov, Birds have paedomorphic dinosaur skulls. *Nature* **487**, 223–226 (2012). doi:10.1038/nature11146 Medline

38. R. J. Butler, A. Goswami, Body size evolution in Mesozoic birds: Little evidence for Cope's rule. *J. Evol. Biol.* **21**, 1673–1682 (2008). doi:10.1111/j.1420-9101.2008.01594.x Medline

39. P. M. O'Connor, A. H. Turner, J. R. Groenke, R. N. Felice, R. R. Rogers, D. W. Krause, L. J. Rahantarisoa, Late Cretaceous bird from Madagascar reveals unique development of beaks. *Nature* **588**, 272–276 (2020). doi:10.1038/s41586-020-2945-x Medline

40. M. Fabbri, G. Navalón, R. B. J. Benson, D. Pol, J. O'Connor, B. S. Bhullar, G. M. Erickson, M. A. Norell, A. Orkney, M. C. Lamanna, S. Zouhri, J. Becker, A. Emke, C. Dal Sasso, G. Bindellini, S. Maganuco, M. Auditore, N. Ibrahim, Subaqueous foraging among carnivorous dinosaurs. *Nature* **603**, 852–857 (2022). doi:10.1038/s41586-022-04528-0 Medline

41. G. A. Klevezal, *Recording Structures of Mammals, Determination of Age and Reconstruction of Life History*. (A. A. Balkema, 1996).

42. M. Köhler, N. Marín-Moratalla, X. Jordana, R. Aanes, Seasonal bone growth and physiology in endotherms shed light on dinosaur physiology. *Nature* **487**, 358–361 (2012). doi:10.1038/nature11264 Medline

43. P. J. Schucht, N. Klein, M. Lambertz, What's my age again? On the ambiguity of histology-based skeletochronology. Proc. *Biol. Sci*. **288**, 20211166 (2021). doi:10.1098/rspb.2021.1166 Medline

44. J. Castanet, H. Francillon-Vieillot, F. J. Meunier, A. de Ricqlès, "Bone and Individual Aging" in *Bone Volume 7: Bone Growth—B*, B. K. Hall Ed. (CRC Press, 1993) vol. 7, chap. 9.

45. N. E. Campione, D. C. Evans, C. M. Brown, M. T. Carrano, Body mass estimation in non-avian bipeds using a theoretical conversion to quadruped stylopodial proportions. *Methods Ecol. Evol.* **5**, 913–923 (2014). doi:10.1111/2041-210X.12226

46. R. B. J. Benson, G. Hunt, M. T. Carrano, N. Campione, Cope's rule and the adaptive landscape of dinosaur body size evolution. *Palaeontology* **61**, 13–48 (2018). doi:10.1111/pala.12329

47. S. J. Nesbitt, J. A. Clarke, A. H. Turner, M. A. Norell, A small alvarezsaurid from the eastern Gobi Desert offers insight into evolutionary patterns in the Alvarezsauroidea. *J. Vertebr. Paleontol.* **31**, 144–153 (2011). doi:10.1080/02724634.2011.540053

48. P. J. Bybee, A. H. Lee, E. T. Lamm, Sizing the Jurassic theropod dinosaur Allosaurus: Assessing growth strategy and evolution of ontogenetic scaling of limbs. *J. Morphol.* **267**, 347–359 (2006). doi:10.1002/jmor.10406 Medline

49. M. A. Loewen, "Variation in the late Jurassic theropod dinosaur *Allosaurus*: ontogenetic, functional, and taxonomic implications," thesis, University of Utah (2009).

50. N. P. Myhrvold, Revisiting the estimation of dinosaur growth rates. *PLOS ONE* **8**, e81917 (2013). doi:10.1371/journal.pone.0081917 Medline

51. L. M. Ibiricu, R. D. Martínez, G. A. Casal, I. A. Cerda, The behavioral implications of a multi-individual bonebed of a small theropod dinosaur. *PLOS* ONE 8, e64253 (2013). doi:10.1371/journal.pone.0064253 Medline

52. T. D. Carr, T. E. Williamson, D. R. Schwimmer, A new genus and species of tyrannosauroid from the Late Cretaceous (Middle Campanian) Demopolis Formation of Alabama. J. *Vertebr. Paleontol.* **25**, 119–143 (2005). doi:10.1671/0272-4634(2005)025[0119:ANGASO]2.0.CO;2

53. C. A. Brochu, Closure of neurocentral sutures during crocodilian ontogeny: Implications for maturity assessment in fossil archosaurs. *J. Vertebr. Paleontol.* **16**, 49–62 (1996). doi:10.1080/02724634.1996.10011283

54. D. C. Evans, P. M. Barrett, K. S. Brink, M. T. Carrano, Osteology and bone microstructure of new, small theropod dinosaur material from the early Late Cretaceous of Morocco. *Gondwana Res.* **27**, 1034–1041 (2015). doi:10.1016/j.gr.2014.03.016

55. A. Lee, Interplay between growth and mechanics in the evolution of bone microstructure in dinosaurs, PhD Dissertation, University of California (2007).

56. A. J. de Ricqlès, K. Padian, J. R. Horner, On the bone histology of some Triassic pseudosuchian archosaurs and related taxa. *Ann. Paleontol.* **89**, 67–101 (2003). doi:10.1016/S0753-3969(03)00005-3

57. S. A. Werning, "Evolution of bone histological characters in amniotes, and the implications for the evolution of growth and metabolism," thesis, University of California (2013).

58. W. L. Parsons, K. M. Parsons, Further descriptions of the osteology of Deinonychus antirrhopus (Saurischia, Theropoda). *Bull. Buffalo Soc. Nat. Sci.* **38**, 43–54 (2009).

59. W. L. Parsons, K. M. Parsons, Morphological variations within the ontogeny of Deinonychus antirrhopus (Theropoda, Dromaeosauridae). *PLOS* ONE **10**, e0121476 (2015). doi:10.1371/journal.pone.0121476 Medline

60. G. M. Erickson, K. Curry Rogers, D. J. Varricchio, M. A. Norell, X. Xu, Growth patterns in brooding dinosaurs reveals the timing of sexual maturity in non-avian dinosaurs and genesis of the avian condition. *Biol. Lett.* **3**, 558–561 (2007). doi:10.1098/rsbl.2007.0254 Medline

61. A. Cau, V. Beyrand, D. F. A. E. Voeten, V. Fernandez, P. Tafforeau, K. Stein, R. Barsbold, K. Tsogtbaatar, P. J. Currie, P. Godefroit, Synchrotron scanning reveals amphibious ecomorphology in a new clade of bird-like dinosaurs. *Nature* **552**, 395–399 (2017). doi:10.1038/nature24679 Medline

62. A. J. de Ricqlès, K. Padian, F. Knoll, J. R. Horner, On the origin of high growth rates in archosaurs and their ancient relatives: Complementary histological studies on Triassic archosauriforms and the problem of a "phylogenetic signal" in bone histology. *Ann. Paleontol.* **94**, 57–76 (2008). doi:10.1016/j.annpal.2008.03.002

63. S. J. Nesbitt, M. D. Ezcurra, The early fossil record of dinosaurs in North America: A new neotheropod from the base of the Upper Triassic Dockum Group of Texas. *Acta Palaeontol. Pol.* **60**, 513–526 (2015). doi:10.4202/app.00143.2014

64. A. H. Lee, P. M. O'Connor, Bone histology confirms determinate growth and small body size in the noasaurid theropod Masiakasaurus knopfleri. *J. Vertebr. Paleontol.* **33**, 865–876 (2013). doi:10.1080/02724634.2013.743898

65. R. E. H. Reid, Zonal "growth rings" in dinosaurs. *Mod. Geol.* **15**, 19–48 (1990).

66. C. Gao, E. M. Morschhauser, D. J. Varricchio, J. Liu, B. Zhao, A second soundly sleeping dragon: New anatomical details of the Chinese troodontid Mei long with implications for phylogeny and taphonomy. *PLOS ONE* **7**, e45203 (2012). doi:10.1371/journal.pone.0045203 Medline

67. P. P. Skutschas, E. A. Boitsova, A. O. Averianov, H.-D. Sues, Ontogenetic changes in long-bone histology of an ornithomimid theropod dinosaur from the Upper Cretaceous Bissekty Formation of Uzbekistan. *Hist. Biol.* **29**, 715–729 (2017). doi:10.1080/08912963.2016.1233180

68. T. M. Cullen, D. C. Evans, M. J. Ryan, P. J. Currie, Y. Kobayashi, Osteohistological variation in growth marks and osteocyte lacunar density in a theropod dinosaur

(Coelurosauria: Ornithomimidae). *BMC Evol. Biol.* **14**, 231 (2014). doi:10.1186/s12862-014-0231-y Medline

69. M. Baiano, I. A. Cerda, Bone microstructure of Quilmesaurus curriei (Theropoda: Abelisauridae). *Pub. Elec. Assn. Pal. Arg.* **18**, R10 (2017).

70. P. C. Sereno, L. Tan, S. L. Brusatte, H. J. Kriegstein, X. Zhao, K. Cloward, Tyrannosaurid skeletal design first evolved at small body size. *Science* **326**, 418–422 (2009). doi:10.1126/science.1177428 Medline

71. D. W. Fowler, H. N. Woodward, E. A. Freedman, P. L. Larson, J. R. Horner, Reanalysis of "Raptorex *kriegsteini*": A juvenile tyrannosaurid dinosaur from Mongolia. *PLOS ONE* 6, e21376 (2011). doi:10.1371/journal.pone.0021376 Medline

72. R. B. J. Benson, N. E. Campione, M. T. Carrano, P. D. Mannion, C. Sullivan, P. Upchurch, D. C. Evans, Rates of dinosaur body mass evolution indicate 170 million years of sustained ecological innovation on the avian stem lineage. *PLOS Biol.* **12**, e1001853 (2014). doi:10.1371/journal.pbio.1001853 Medline

73. B. McFeeters, M. J. Ryan, C. Schröder-Adams, T. M. Cullen, A new ornithomimid theropod from the Dinosaur Park Formation of Alberta, Canada. J. *Vertebr. Paleontol.* **36**, e1221415 (2016). doi:10.1080/02724634.2016.1221415

74. R. E. H. Reid, Apparent zonation and slowed late growth in a small Cretaceous theropod. *Mod. Geol.* **18**, 391–406 (1993).

75. T. M. Lehman, "Growth and population age structure in the horned dinosaur *Chasmosaurus*" in *Horns and Beaks: Ceratopsian and Ornithopod Dinosaurs*, K. Carpenter, Ed. (IU press, 2006), pp. 259–317.

76. D. J. Varricchio, P. C. Sereno, Z. Xi-jin, T. Lin, J. A. Wilson, G. H. Lyon, Mud-trapped herd captures evidence of distinctive dinosaur sociality. *Acta Palaeontol. Pol.* **53**, 567–578 (2008). doi:10.4202/app.2008.0402

77. A. Chinsamy, T. H. Rich, P. Vickers-Rich, Polar dinosaur bone histology. *J. Vertebr. Paleontol.* **18**, 385–390 (1998). doi:10.1080/02724634.1998.10011066

78. K. Waskow, O. Mateus, Dorsal rib histology of dinosaurs and a crocodylomorph from western Portugal: Skeletochronological implications on age determination and life history traits. *C. R. Palevol* **16**, 425–439 (2017). doi:10.1016/j.crpv.2017.01.003

79. J. R. Horner, K. Padian, Age and growth dynamics of *Tyrannosaurus rex*. *Proc. Biol. Sci.* **271**, 1875–1880 (2004). doi:10.1098/rspb.2004.2829 Medline

80. G. A. de Souza, M. B. Soares, A. S. Brum, M. Zucolotto, J. M. Sayão, L. C. Weinschütz, A. W. A. Kellner, Osteohistology and growth dynamics of the Brazilian noasaurid Vespersaurus paranaensis Langer et al., 2019 (Theropoda: Abelisauroidea). *PeerJ* **8**, e9771 (2020). Medline

81. G. M. Erickson, T. A. Tumanova, Growth curve of Psittacosaurus mongoliensis Osborn (Ceratopsia: Psittacosauridae) inferred from long bone histology. Zool. J. Linn. Soc. 130, 551–566 (2000). doi:10.1111/j.1096-3642.2000.tb02201.x

82. C. A. Brassey, S. C. R. Maidment, P. M. Barrett, Body mass estimates of an exceptionally complete Stegosaurus (Ornithischia: Thyreophora): comparing volumetric and linear

bivariate mass estimation methods. *Biol. Lett.* **11**, 20140984 (2015). doi:10.1098/rsbl.2014.0984 Medline

83. X. Xu, J. Choiniere, Q. Tan, R. B. J. Benson, J. Clark, C. Sullivan, Q. Zhao, F. Han, Q. Ma, Y. He, S. Wang, H. Xing, L. Tan, Two early Cretaceous fossils document transitional stages in Alvarezsaurian dinosaur evolution. *Curr. Biol.* **28**, 2853–2860.e3 (2018). doi:10.1016/j.cub.2018.07.057 Medline

84. R. Delcourt, O. N. Grillo, Tyrannosauroids from the Southern Hemisphere: Implications for biogeography, evolution, and taxonomy. *Palaeogeogr. Palaeoclimatol. Palaeoecol.* **511**, 379–387 (2018). doi:10.1016/j.palaeo.2018.09.003

85. F. E. Novas, F. L. Agnolín, M. D. Ezcurra, J. Porfiri, J. I. Canale, Evolution of the carnivorous dinosaurs during the Cretaceous: The evidence from Patagonia. *Cretac. Res.* **45**, 174–215 (2013). doi:10.1016/j.cretres.2013.04.001

86. M. C. Langer, N. O. Martins, P. C. Manzig, G. S. Ferreira, J. C. A. Marsola, E. Fortes, R. Lima, L. C. F. Sant'ana, L. D. S. Vidal, R. H. D. S. Lorençato, M. D. Ezcurra, A new desert-dwelling dinosaur (Theropoda, Noasaurinae) from the Cretaceous of south Brazil. *Sci. Rep.* **9**, 9379 (2019). doi:10.1038/s41598-019-45306-9 Medline

87. O. W. M. Rauhut, D. Pol, Probable basal allosauroid from the early Middle Jurassic Cañadón Asfalto Formation of Argentina highlights phylogenetic uncertainty in tetanuran theropod dinosaurs. *Sci. Rep.* **9**, 18826 (2019). doi:10.1038/s41598-019-53672-7 Medline

88. M. D. D'Emic, P. D. Mannion, P. Upchurch, R. B. J. Benson, Q. Pang, C. Zhengwu, Osteology of Huabeisaurus allocotus (Sauropoda: Titanosauriformes) from the Upper Cretaceous of China. *PLOS ONE* **8**, e69375 (2013). doi:10.1371/journal.pone.0069375 Medline

89. O. Hammer, D. A. Harper, P. D. Ryan, PAST: Paleontological statistics software package for education and data analysis. Palaeontol. *Electronica* **4**, 1–9 (2001).

90. L. J. Revell, Phytools: An R package for phylogenetic comparative biology (and other things). *Methods Ecol. Evol.* **3**, 217–223 (2012). doi:10.1111/j.2041-210X.2011.00169.x

91. B. M. Kilbourne, P. J. Makovicky, Limb bone allometry during postnatal ontogeny in non-avian dinosaurs. *J. Anat.* **217**, 135–152 (2010). doi:10.1111/j.1469-7580.2010.01253.x Medline

92. J. H. Madsen Jr., S. P. Welles, Ceratosaurus (Dinosauria, Theropoda) a revised osteology. *Utah Geological Survey* **2**, 1–80 (2000).

93. M. T. Carrano, R. B. J. Benson, S. D. Sampson, The phylogeny of Tetanurae (Dinosauria: Theropoda). J. Syst. *Palaeontology* **10**, 211–300 (2012). doi:10.1080/14772019.2011.630927

94. R. E. H. Reid, Bone histology of the Cleveland-Lloyd dinosaurs and of dinosaurs in general. *Geol. Stud.* **41**, 25–71 (1996).

95. M. H. Schweitzer, W. Zheng, L. Zanno, S. Werning, T. Sugiyama, Chemistry supports the identification of gender-specific reproductive tissue in Tyrannosaurus rex. *Sci. Rep.* **6**, 23099 (2016). doi:10.1038/srep23099 Medline

96. R. Redelstorff, S. Hayashi, B. Rothschild, A. Chinsamy-Turan, Non-traumatic bone infection in stegosaurs from Como Bluff, Wyoming. *Lethaia* **48**, 47–55 (2015). doi:10.1111/let.12086

97. A. Chinsamy, A. Tumarkin-Deratzian, Pathologic bone tissues in a Turkey vulture and a nonavian dinosaur: Implications for interpreting endosteal bone and radial fibrolamellar bone in fossil dinosaurs. *Anat. Rec.* **292**, 1478–1484 (2009). doi:10.1002/ar.20991 Medline

98. M. T. Carrano, J. R. Hutchinson, Pelvic and hindlimb musculature of Tyrannosaurus rex (Dinosauria: Theropoda). *J. Morphol.* **253**, 207–228 (2002). doi:10.1002/jmor.10018 Medline

99. P. M. Sander, Longbone histology of the Tendaguru sauropods: Implications for growth and biology. *Paleobiology* **26**, 466–488 (2000). doi:10.1666/0094-8373(2000)026<0466:LHOTTS>2.0.CO;2

100. J. R. Horner, A. de Ricqlès, K. Padian, Long bone histology of the hadrosaurid dinosaur Maiasaura peeblesorum: Growth dynamics and physiology based on an ontogenetic series of skeletal elements. *J. Vertebr. Paleontol.* **20**, 115–129 (2000). doi:10.1671/0272-4634(2000)020[0115:LBHOTH]2.0.CO;2

101. N. Ibrahim, P. C. Sereno, C. Dal Sasso, S. Maganuco, M. Fabbri, D. M. Martill, S. Zouhri, N. Myhrvold, D. A. Iurino, Semiaquatic adaptations in a giant predatory dinosaur. *Science* **345**, 1613–1616 (2014). doi:10.1126/science.1258750 Medline

102. T. Tsuihiji, M. Watabe, K. Togtbaatar, T. Tsubamoto, R. Barsbold, S. Suzuki, A. H. Lee, R. C. Ridgely, Y. Kawahara, L. M. Witmer, Cranial osteology of a juvenile specimen of Tarbosaurus bataar (Theropoda, Tyrannosauridae) from the Nemegt Formation (Upper Cretaceous) of Bugin Tsav, Mongolia. J. *Vertebr. Paleontol.* **31**, 497–517 (2011). doi:10.1080/02724634.2011.557116

103. H. N. Woodward, T. H. Rich, A. Chinsamy, P. Vickers-Rich, Growth dynamics of Australia's polar dinosaurs. *PLOS ONE* **6**, e23339 (2011). doi:10.1371/journal.pone.0023339 Medline

104. D. J. Varricchio, Bone microstructure of the Upper Cretaceous theropod dinosaur Troodon formosus. *J. Vertebr. Paleontol.* 13, 99–104 (1993). doi:10.1080/02724634.1993.10011490

105. D. J. Varricchio, J. R. Moore, G. M. Erickson, M. A. Norell, F. D. Jackson, J. J. Borkowski, Avian paternal care had dinosaur origin. *Science* **322**, 1826–1828 (2008). doi:10.1126/science.1163245 Medline